Flux pinning and phase transitions in model high-temperature superconductors with columnar defects

K. H. Lee and D. Stroud
Department of Physics, Ohio State University, Columbus, Ohio 43210

S. M. Girvin
Department of Physics, Indiana University, Bloomington, Indiana 47405
(Received 3 December 1992; revised manuscript received 23 February 1993)

We calculate the degree of flux pinning by defects in model high-temperature superconductors (HTSC's). The HTSC is modeled as a three-dimensional network of resistively shunted Josephson junctions in an external magnetic field, corresponding to a HTSC in the extreme type-II limit. Disorder is introduced either by randomizing the coupling between grains (model-A disorder) or by removing grains (model-B disorder). Three types of defects are considered: point disorder, random line disorder, and periodic line disorder; but the emphasis is on random line disorder. Static and dynamic properties of the models are determined by Monte Carlo simulations and by solution of the analogous coupled overdamped Josephson equations in the presence of thermal noise. Random line defects considerably raise the superconducting transition temperature $T_c(B)$, and increase the apparent critical current density $J_c(B,T)$, in comparison to the defect-free crystal. They are more effective in these respects than a comparable volume density of point defects, in agreement with the experiments of Civale *et al.* Periodic line defects commensurate with the flux lattice are found to raise $T_c(B)$ even more than do random line defects. Random line defects are most effective when their density approximately equals the flux density. Near $T_c(B)$, our static and dynamic results appear consistent with the anisotropic Bose-glass-scaling hypotheses of Nelson and Vinokur, but with possibly different critical indices.

I. INTRODUCTION

A major problem restricting the practical use of high-temperature superconductors (HTSC's) is the difficulty of producing a large critical current, especially in a magnetic field.[1] Much of this difficulty is thought to result from dissipation due to flux motion—a dissipation generally known at low or high dissipation rates as "flux creep"[2–6] or "flux flow,"[7] respectively. When a current density **J** is introduced into the HTSC, it produces a $\mathbf{J}\times\mathbf{B}$ force (known as a Magnus force) on the flux lines. This force tends to set the lines in motion, producing resistive dissipation, unless appropriate defects, known as pinning centers, can prevent this motion, or at least raise the current density at which it begins.

Recently, Civale *et al.*,[8] in an elegant set of experiments, have shown that columnar defects, introduced parallel to the flux lines by heavy ion irradiation, can greatly increase the critical current at which flux motion dissipation begins, relative to the point defects which are more commonly introduced as pinning centers, e.g., by proton irradiation.[9–11] The same columnar defects were also found to increase the temperature of the so-called "irreversibility line"[12] in the magnetic-field–temperature (H-T) plane, below which flux motion essentially ceases in the limit of a weak applied current. The columnar pins were produced by irradiating the HTSC with a beam of heavy ions parallel to the c axis. It is not surprising that columnar defects should be effective pins: they provide a long pinning center which should provide a much stronger pinning potential for a long flux line than will an equal concentration of point defects. However, a realistic calculation which demonstrates this effect has been lacking.

In this paper we present some simple model calculations which demonstrate both of the effects observed by Civale *et al.*,[8] and also suggest some alternative methods for further increasing both the critical current and irreversibility temperature of HTSC's. Our approach is to describe the HTSC as a three-dimensional collection of resistively shunted Josephson junctions (RSJ's), in which temperature is simulated by a Langevin noise source of the appropriate strength in each junction.[13] Such a model is obviously far from a realistic HTSC. However, the model does contain some of the essential physics needed to describe transport in HTSC's: it embodies coupled fluctuating phases within the context of a reasonable dynamics, and it allows for the introduction of an applied magnetic field in a simple way. In this view, the Josephson-coupled "grains" should probably be considered as representing small patches of phase-coherent superconductor, of dimensions comparable to the coherence length.[14] Thus the model is not restricted to literally granular materials, but could apply to single crystals with more microscopic disorder, in the extreme type-II limit (penetration depth λ much larger than coherence length ξ). We have shown elsewhere that a similar model describes the difference between transverse and longitudinal magnetoresistance of a HTSC, in qualitative agreement with experiment.[15]

We turn now to the body of the paper. Section II describes the model for both the thermodynamic and trans-

port properties of the HTSC with defects. Section III describes our numerical results for these properties. A brief discussion follows in Sec. IV. Three appendices summarize the static and dynamic scaling hypotheses used to analyze our numerical results.

II. MODEL

A. Thermodynamics

We consider a simple cubic three-dimensional network of N superconducting "grains" weakly coupled together by Josephson junctions, and derived by an externally applied current. The ith "grain" is described by a superconducting order parameter $|\psi_i|\exp(i\theta_i)$. We neglect fluctuations in the amplitude $|\psi_i|$ and allow the phase θ_i to fluctuate. With these assumptions, the thermodynamic properties of the network are given by the Hamiltonian

$$H=-\sum_{\langle ij\rangle} E_{J;ij}\cos(\theta_i-\theta_j-A_{ij}) , \tag{1}$$

where

$$E_{J;ij}\equiv\frac{\hbar}{2e}I_{c;ij} \tag{2}$$

is the coupling energy between grains i and j, $I_{c;ij}$ is the corresponding critical current,

$$A_{ij}=\frac{2\pi}{\Phi_0}\int_i^j \mathbf{A}\cdot\mathbf{dl} , \tag{3}$$

$\Phi_0=hc/2e$, and $\mathbf{A}$ is the vector potential, taken to be that of the externally applied magnetic field (this is equivalent to assuming a Josephson penetration depth large compared to the intergranular separation). The sum runs over distinct nearest-neighbor pairs.

Given H, equilibrium properties are obtained via an average with respect to a canonical ensemble. Thus, for example, the average of some operator $O(\theta_1,\ldots,\theta_N)$ is obtained from

$$\langle O\rangle=\int O(\theta_1,\ldots,\theta_N)e^{-H(\theta_1,\ldots,\theta_N)/k_BT}\prod_{i=1}^{N}d\theta_i/Z , \tag{4}$$

where

$$Z=\int\prod_i d\theta_i\exp(-H/k_BT) \tag{5}$$

is the canonical partition function.

In the calculations to be described below, we have generally dealt with *disordered* samples. In that case, we calculate averages both over a canonical ensemble (denoted $\langle\ \rangle$) and over different realizations of the disorder (denoted [ ]). We have considered primarily the specific heat per grain C_V and the so-called helicity modulus tensor with components γ_{ij}. C_V is generally computed from the fluctuation expression

$$C_V=[\langle H^2\rangle-\langle H\rangle^2]/(Nk_BT^2) . \tag{6}$$

The helicity modulus (or equivalently, the superfluid density) is the free energy cost of imposing a twist in the phase at the boundaries of the sample. Its principal elements are essentially spin-wave stiffness constants. Rather than imposing a twisted boundary condition and calculating the resulting increase in free energy, it is more convenient to use periodic boundary conditions and calculate γ_{ij} as

$$\gamma_{ij}=\left[\frac{\partial^2 F}{\partial A_i'\partial A_j'}\right]_{\mathbf{A}'=0} . \tag{7}$$

Here $\mathbf{A}'$ represents an added uniform vector potential (in addition to that which produces the applied magnetic field) which is included in the Hamiltonian in order to produce a twist. The various second derivatives in Eq. (7) are readily computed explicitly for an ordered or a disordered sample, with the result for, e.g., γ_{xx}:

$$\begin{aligned}N\gamma_{xx}=&\left[\left\langle\sum_{\langle ij\rangle}E_{J;ij}x_{ij}^2\cos(\theta_i-\theta_j-A_{ij})\right\rangle\right]\\&-\frac{1}{k_BT}\left[\left\langle\left[\sum_{\langle ij\rangle}E_{J;ij}x_{ij}\sin(\theta_i-\theta_j-A_{ij})\right]^2\right\rangle\right]\\&+\frac{1}{k_BT}\left[\left\langle\sum_{\langle ij\rangle}E_{J;ij}x_{ij}\sin(\theta_i-\theta_j-A_{ij})\right\rangle^2\right] ,\end{aligned} \tag{8}$$

where $x_{ij}=x_j-x_i$ is the x coordinate of the distance between nearest-neighbor grains i and j. Similar expressions hold for the other components of γ.[16,17]

B. Dynamics

There are many dynamical models whose equilibrium thermodynamic properties are represented by the model just described. We choose a dynamical model corresponding to a simple cubic array of overdamped resistively shunted Josephson junctions, driven by an applied current. The network is then characterized by the set of coupled equations

$$I_{ij}=I_c\sin(\theta_i-\theta_j-A_{ij})+\frac{V_{ij}}{R_{ij}}+I_{L;ij} , \tag{9}$$

$$V_{ij}\equiv V_i-V_j=\frac{\hbar}{2e}\frac{d}{dt}(\theta_i-\theta_j) , \tag{10}$$

$$\sum_j I_{ij}=I_{i;\mathrm{ext}} , \tag{11}$$

$$A_{ij}=\frac{2\pi}{\Phi_0}\int_{\mathbf{x}_i}^{\mathbf{x}_j}\mathbf{A}\cdot\mathbf{dl} . \tag{12}$$

Here I_{ij} is the current from grain i to grain j, which is written as the sum of a Josephson current and an Ohmic current through the shunt resistance R_{ij}; V_{ij} is the voltage difference between grains i and j; and $I_{i;\mathrm{ext}}$ is the external current fed into grain i. In the calculations described below, the current is always fed into one face of the array (an equal amount I into each grain) and extracted from the opposite face, with periodic transverse boundary conditions. Equation (11) is Kirchhoff's law describing current conservation at grain i. $I_{L;ij}$ is a Langevin noise current[18] between grains i and j, introduced to simulate the effects of temperature, which

satisfies the relation

$$\langle I_{L;ij}(t)\rangle = 0 , \tag{13}$$

$$\langle I_{L;ij}(t) I_{L;kl}(t')\rangle = \frac{2k_B T}{R_{ij}} \delta_{ij;kl}\delta(t-t') , \tag{14}$$

where T is the absolute temperature and the brackets denote an ensemble average. We solve these equations by Euler iteration, as described previously.[13,15]

C. Geometrical models for line and point disorder

We have considered two types of models to describe disorder, which we denote models A and B. In model A, the bond energy $E_{J;ij}$ between grains i and j is assumed to vary randomly between 0 and twice its average value. In model B, we introduce disorder simply by removing a certain fraction of the grains, as well as their associated Josephson junctions (but not shunt resistances).

For either model A or B, we can assume either "line disorder" or "point disorder." In model A, point disorder can be introduced by assuming that the bond strengths of different bonds are completely uncorrelated. "Line disorder" consists of assuming that the bond strengths are uncorrelated in the xy plane, but are perfectly correlated in the z direction—that is, the strength of a given bond, whatever its orientation, depends on the x and y coordinates describing its location, but not on the z coordinate.

To introduce point disorder in model B, we remove the grains at random. For line disorder, we remove lines of grains parallel to the z axis. The removal of these grains effectively converts the neighborhood of the grain from superconducting to normal. In model B, we have also considered "periodic line disorder," in which line defects are arranged periodically in the xy plane, as described further below.

D. Magnetic field

We consider magnetic fields applied in the z direction, i.e., parallel to the line defects. In previous calculations of this sort, it has been standard to use the Landau gauge, $\mathbf{A}=Bx\hat{\mathbf{y}}$. This gauge severely restricts the possible magnetic fields that can be considered if one also requires periodic boundary conditions in all three directions (as in the Monte Carlo simulations) or in the transverse directions (as with the dynamic simulations). We have therefore used a different gauge previously used by Arovas and Haldane in other contexts.[19]

To define this gauge, we consider an $L\times L$ square array of lattice constant a, with the origin taken as the lower left-hand corner of the array. Then we take $A_{ij}=2\pi fn$ for bonds pointing in the y direction and located at $x=na$; $A_{ij}=0$ for all bonds in the x direction except for those in the extreme right-hand column of plaquettes, and $A_{ij}=-2\pi fLm$ for horizontal bonds in that extreme right-hand column, at $y=ma$, $x=La$. (In this expression $f=\Phi/\Phi_0$, where Φ is the flux per plaquette.) With this choice of gauge, it is readily verified that the factors A_{ij} sum to $2\pi f$ (modulo 2π) around each plaquette, as required. The requirement of periodicity in the two transverse directions will now be satisfied as long as f is a multiple of $1/L^2$. This is much weaker than the condition imposed by periodicity when the Landau gauge is used, which is that f be a multiple of $1/L$.

The reader may be concerned that the line integral of the vector potential along noncontractible loops in both directions around the torus varies with position in this gauge. This, however, is physically correct: it is a consequence of the noncommutativity of translations in the presence of a magnetic field. Consider, for instance, the usual continuum problem in the Landau gauge. The lowest Landau level eigenfunctions are plane waves in the y direction and Gaussians in the x direction whose peak position is proportional to the y momentum

$$\phi_k(x,y)=e^{iky}\exp[-(x-kl^2)^2/2l^2] ,$$

where l is the magnetic length.[20] Because y momentum is coupled to x position, one is forced to use generalized periodic boundary conditions. That is, one has periodic boundary conditions in the y direction, but there is a phase discontinuity at the x boundary whose magnitude is proportional to y. This same need to generalize the boundary conditions also occurs on the lattice in the cases where fL is not an integer. However, on the discrete lattice, we can convert to periodic boundary conditions in both directions by replacing the boundary angle twist with a vector potential in the horizontal bonds in the extreme right-hand column. This is the procedure we have adopted here; it is equivalent to the standard procedure in the continuum. This subtlety is irrelevant to our present results since it happens that we have carried out our static calculations at values of the flux such that fL is an integer. For the dynamic calculations we have imposed only the weaker condition $fL^2=$integer, but have free boundary conditions on the sample faces perpendicular to the direction of the current injection. Yu, Lee, and Stroud[13] have shown that the use of this gauge to calculate IV characteristics at fields such that $fL^2=1$ leads to excellent agreement with expected behavior in a two-dimensional array of Josephson junctions.

III. NUMERICAL RESULTS

A. Model A

We begin by presenting our numerical results for model A. Figure 1 shows the specific heat C_V per grain and the helicity moduli $\gamma_\parallel$ and $\gamma_\perp$ parallel and perpendicular to the magnetic field, for an ordered array of size $L\times L\times L$ grains with periodic boundary conditions, isotropic coupling, magnetic field $f=\frac{1}{4}$, and several different sizes ($L=8$, 12, and 16). C_V shows clear signs of diverging in the vicinity of $k_BT=1.1E_J$ (the peak in C_V is growing with increasing lattice size, suggesting a continuous phase transition). We interpret this temperature as a melting transition with a discrete symmetry associated with the periodic lattice. Similar numerical results have been obtained for this model by Shih, Ebner, and Stroud[17] and by Hetzel, Sudbo, and Huse.[21]

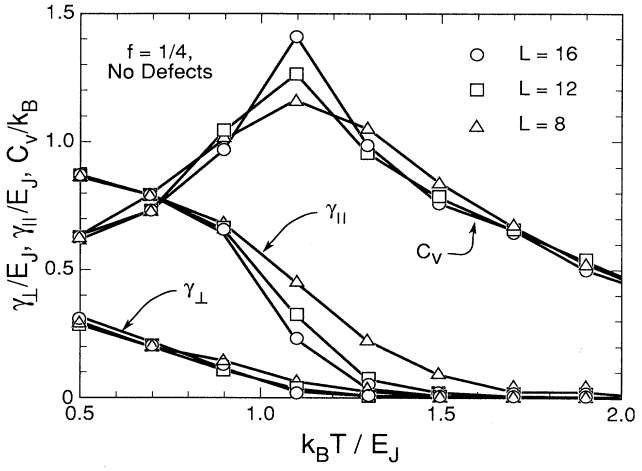

FIG. 1. Specific heat per grain, C_V; and parallel and perpendicular components of the helicity moduli, $\gamma_{\parallel}$ and $\gamma_{\perp}$, for an ordered $L\times L\times L$ lattice of grains, with isotropic coupling ($E_{J,\perp}=E_{J,\parallel}\equiv E_J$), magnetic field $f=\frac{1}{4}$, and $L=8$, 12, and 16, with periodic boundary conditions, plotted as a function of temperature T.

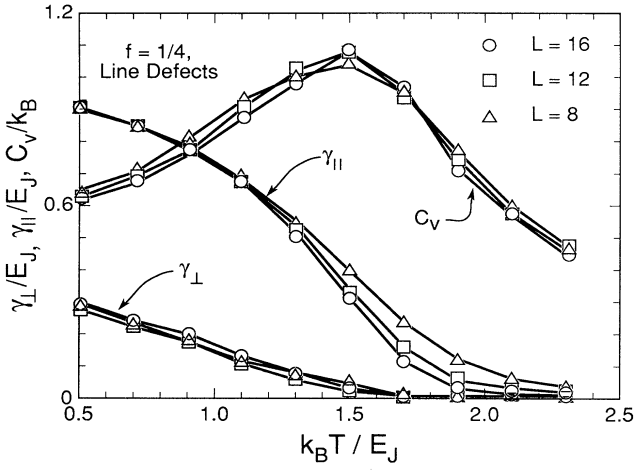

FIG. 3. Same as Fig. 1, but for an array with model-A line disorder in the bond strengths. The calculations involve averages over 35, 21, and 19 realizations of the disorder for $L=8$, 12, and 16, respectively.

We have attempted to get a clearer quantitative picture of this phase transition by applying a static scaling analysis,[22–24,16] as described in detail in Appendix A. In Fig. 2, we plot $L\gamma_{\parallel}$ and $L\gamma_{\perp}$ for several values of L as a function of temperature. As is clear from the figure, each attains a universal value near the same temperature $k_BT_c=1.1E_J$, suggesting that this is indeed the critical temperature for this model. When combined with the scaling analysis of Appendix A, these results suggest that this phase transition is characterized by a single correlation length ξ, i.e., $z=1$, where z is the anisotropy exponent, defined by the relation $\xi_{\parallel}\propto\xi_{\perp}^{z}$, where $\xi_{\parallel}$ and $\xi_{\perp}$ are the correlation lengths parallel and perpendicular to the field.

Figure 3 shows the quantities of Fig. 1, but with line disorder.[25] Once again, we consider isotropic coupling strengths and use $f=\frac{1}{4}$, and several different (but cubic) box sizes. The calculations shown are the result of averages over many realizations of the disorder, as indicated in the legends of the figure. In contrast to Fig. 1, there is very little size dependence of C_V, suggesting that C_V either does not diverge or at most diverges very weakly. Note also that the helicity modulus $\gamma_{\perp}$ goes to zero at a substantially higher temperature than in the ordered case, indicating that the superconducting transition temperature is increased by the line disorder.

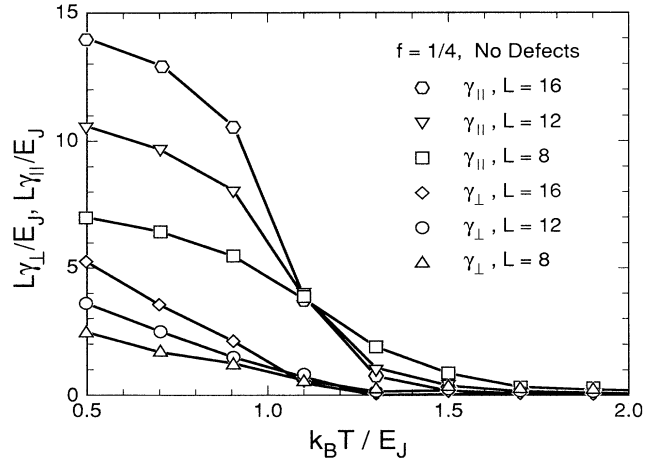

FIG. 2. $L\gamma_{\parallel}$ and $L\gamma_{\perp}$ vs temperature, for the array of Fig. 1.

Another point is that, like the ordered case, $\gamma_{\parallel}$ also seems to vanish continuously with temperature. If we assume a power law of the form $\gamma_{\parallel}\propto|T-T_c|^{g_{\parallel}}$, then Fig. 3 suggests $0<g_{\parallel}<1.0$ [a consequence of the downward concavity of $\gamma_{\parallel}(T)$] and $k_BT_c\approx 1.7E_J$. The numerical uncertainties in $\gamma_{\perp}$ are much larger, so any estimate of the analogous quantity $g_{\perp}$ is difficult. Indeed, at any given temperature, the Monte Carlo convergence of $\gamma_{\perp}$ is much slower than for $\gamma_{\parallel}$. This is presumably because our model is both frustrated and disordered in the xy plane, but is neither frustrated nor ordered in the z direction. Hence the system rapidly responds to any twist in that direction, but much more slowly in the xy plane. Also, $\gamma_{\perp}$ converges more slowly in the disordered case than in the frustrated but ordered model of Fig. 1, suggesting that the slow convergence is caused by the huge number of metastable states of nearly equal energy which are expected in the disordered system.

From the static scaling analysis of Appendix A, we can place tentative limits on the anisotropy exponent z defined there.[22] From Eq. (A7) of Appendix A, $g_{\parallel}=\nu_{\perp}(2-z)$, where $\nu_{\perp}$ is related to the transverse correlation length $\xi_{\perp}$ by $\xi_{\perp}\propto|(T-T_c)/T_c|^{-\nu_{\perp}}$. If we assume that $\gamma_{\parallel}$ goes continously to zero, rather than exhibiting an abrupt jump, then our numerical results would suggest

$$\nu_{\perp}(2-z)>0\ . \tag{15}$$

If $\nu_\perp$ is finite, this inequality suggests that $z<2$ for this model. Secondly, since C_V is apparently nondivergent, Eq. (A5) shows that

$$(2+z)\nu_\perp \geq 2 \ . \tag{16}$$

Adding these results, we get $4\nu_\perp \geq 2$ or $\nu_\perp \geq 0.5$. Hence $(2-z)=0.5/\nu_\perp \leq 1$ or $z \geq 1$. Combining all these arguments, we suggest $1 \leq z \leq 2$. Of course, all these estimates are based on the assumption, not conclusively proven by our numerical results, that there really is a continuous phase transition in the disordered system characterized by static critical phenomena.

In order to go further, we would need to estimate $g_\perp$. According to Eq. (A8) of Appendix A, $g_\perp = z\nu_\perp$. From Fig. 3, we can say little about $g_\perp$ other than to postulate, on the basis of the numerical results, that $\gamma_\perp$ is concave upward, which would give $z\nu_\perp > 1$. Thus we are reluctant to further narrow our estimate $1<z<2$. Presumably, the value of $\nu_\perp$ for this model will agree with the results of Chayes *et al.*,[26] who have proposed, for a wide class of continuous-spin models with disorder, that $\nu_\perp \geq 1$ rigorously.

We turn now to the dynamical properties of model *A*, concentrating on isotropic coupling with and without line disorder. Figure 4 shows the *IV* characteristics of a $6\times6\times9$ array at magnetic field $f=\frac{1}{4}$, with no defects and with current density $\mathbf{J}\perp\mathbf{B}$, plotted at several different temperatures. Figures 5(a) and 5(b) shows the *IV* characteristics for the analogous model with line disorder, a $6\times6\times6$ unit cell, and two current orientations: $\mathbf{J}\perp\mathbf{B}$ and $\mathbf{J}\parallel\mathbf{B}$. Like the Monte Carlo results, the *IV* characteristics also suggest that T_c is increased by line defects. To make this clearer, we have plotted in Fig. 6 the resistivity $\rho \equiv \langle V \rangle /(LRI)$ at a current level $I=0.05I_c$: the introduction of line defects reduces ρ at every temperature, relative to the no-defect case.

The shape of the *IV* characteristics is also changed by

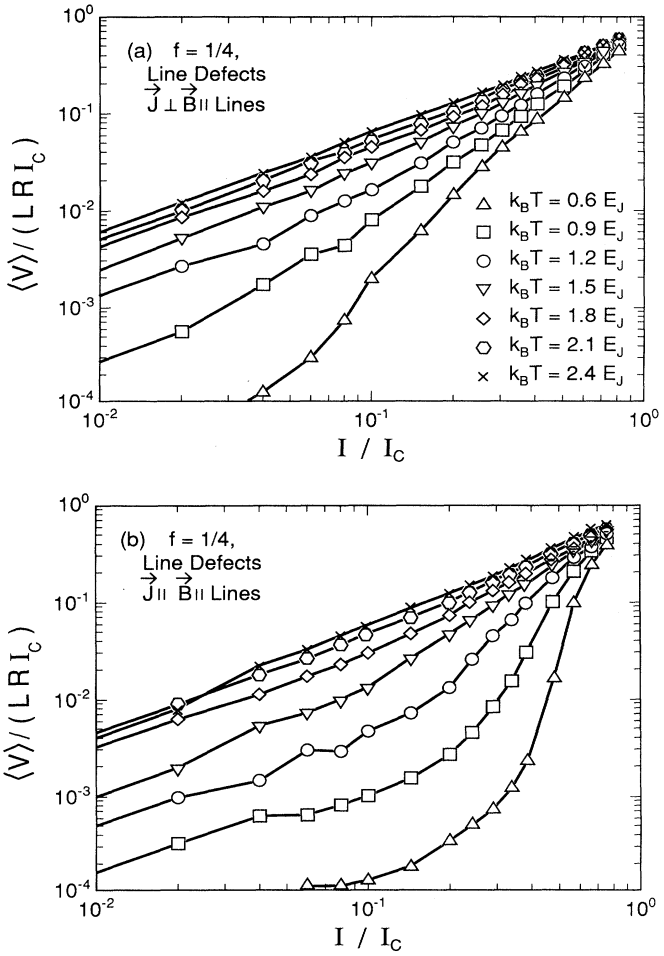

FIG. 5. *IV* characteristics for the model of Fig. 3, $L\times L\times L$ array, with $L=6$: (a) $\mathbf{J}\perp\mathbf{B}$, and (b) $\mathbf{J}\parallel\mathbf{B}$, at several different temperatures, as indicated.

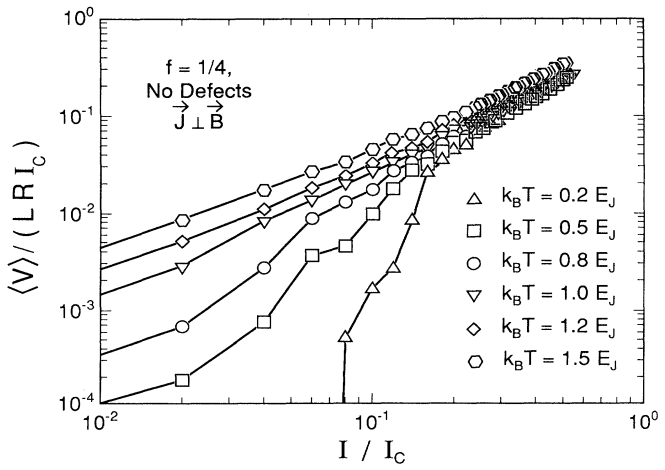

FIG. 4. *IV* characteristics for the model of Fig. 1, $L\times L\times L_z$ array, current density $\mathbf{J}\perp\mathbf{B}$, at several different temperatures, averaged over three different (random) choices of initial conditions, and $L=6$, $L_z=9$. In this and subsequent figures, the lines are simply interpolations between calculated points.

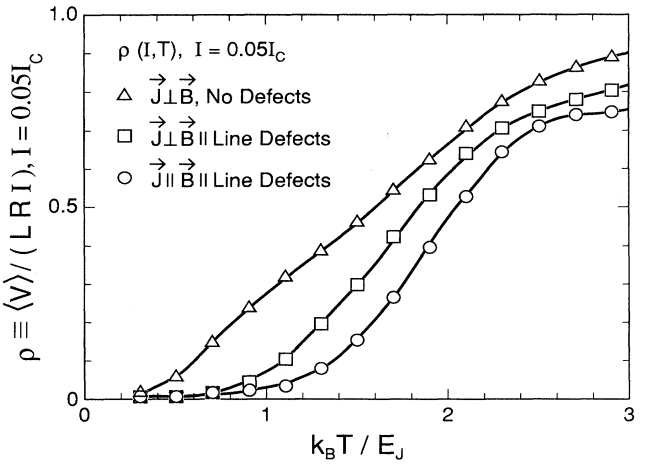

FIG. 6. Resistivity $\rho \equiv \langle V \rangle /(LRI)$ for an $L\times L\times L$ array with $L=6$, at a current level $I=0.05I_c$ per grain, for $f=\frac{1}{4}$ and no defects, $\mathbf{J}\perp\mathbf{B}$ (triangles); line defects, $\mathbf{J}\perp\mathbf{B}$ (squares); and line defects, $\mathbf{J}\parallel\mathbf{B}$ (circles). Cases for line defects involve averages over ten realizations of the disorder.

the introduction of line defects. With no line defects and **J⊥B** (Fig. 4), there is a fairly clear critical current onset for temperatures $k_B T < 1.0 E_J/k_B$. When line defects are present, the *IV* characteristics suggest no clear critical current for **J⊥B** (the analytic form of the *IV* characteristics is discussed further below). By contrast, for **J‖B**, a critical current seems to develop for $k_B T < (1.3-1.4) E_J$.

We have attempted to scale the *IV* characteristics of Fig. 5 according to the formalism[23] outlined in Appendix B. For **J⊥B**, we plot $E_\perp t^{-\nu_\perp(1+z')}$ against $J_\perp t^{-\nu_\perp(1+z)}$ (where $t = |T - T_c|/T_c$) for various estimates of T_c, z, z', and $\nu_\perp$. For **J‖B**, we plot $E_\parallel t^{-\nu_\perp(z+z')}$ against $J_\parallel t^{-2\nu_\perp}$. Our best results are shown in Figs. 7(a) and 7(b); the fitting parameters are shown in the captions, but should not be taken too seriously in view of the numerical uncertainties, small sample sizes, and limited current ranges.

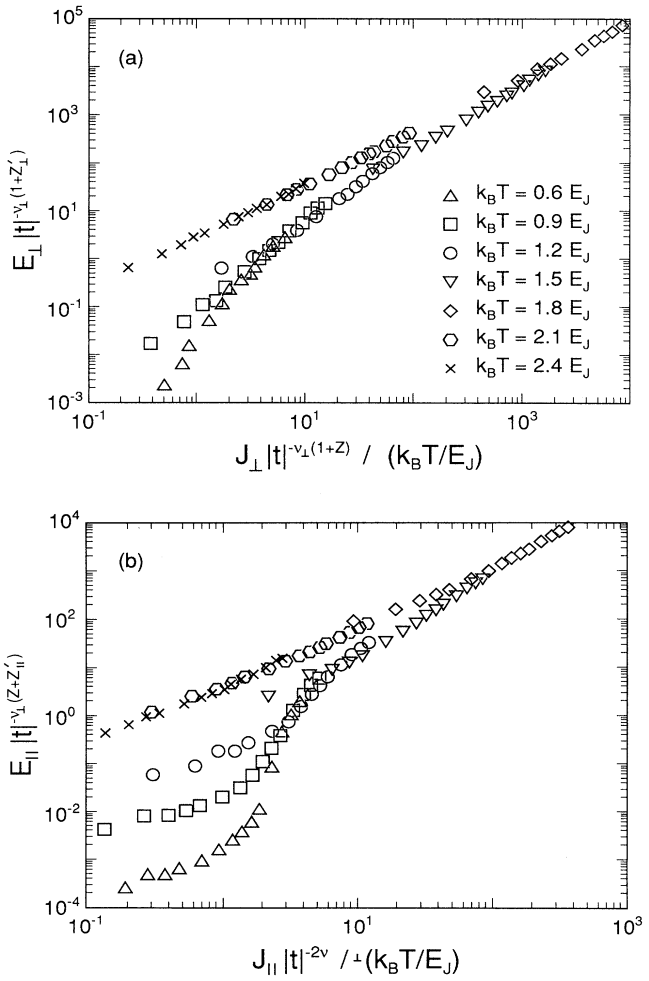

FIG. 7. Scaling plots of the *IV* characteristics from Fig. 5 for (a) **J⊥B** and (b) **J‖B**. In both cases, the *IV* characteristics both above and below $T_c(B)$ collapse reasonably well onto universal scaling functions over the limited current ranges considered. For $T < T_c$, there are low-current Ohmic tails in both cases (especially for **J‖B**), which are probably due to finite-size effects. The fitting parameters for curves (a) are $z = 1.5$, $z' = 2.0$, $\nu_\perp = 1.5$, $k_B T_c = 1.7 E_J$; for curves (b), they are $z = 1.5$, $z' = 1.3$, $\nu_\perp = 1.2$, and $k_B T_c = 1.7 E_J$.

For a given choice of T_c, the best fits seem to correspond to somewhat different values of the parameters in the parallel and perpendicular directions—a result also found by Wallin and Girvin[27] in the case of short-range interactions between vortex lines. Both above and below the assumed T_c, the *IV* characteristics in both the parallel and perpendicular cases collapse adequately (though not perfectly) onto hypothetical universal scaling functions above and below T_c. For both current directions, but especially for **J‖B**, there is a conspicuous Ohmic tail in the *IV* characteristics below T_c. We believe this is a finite-size effect, as further analyzed in Appendix C. Indeed, we have checked that the tail becomes smaller and smaller as the size of the array is increased. When $T < T_c$, the perpendicular and parallel scaling functions are quite dissimilar. In both cases, we can obtain acceptable fits with scaling functions of the form $E(x) \propto \exp[-(A/x)^\mu]$, but the best fit for $\mu_\perp$ is in the range 0.2–0.4 while $\mu_\parallel \approx 1$. This is consistent with the *IV* characteristics of Fig. 5, which show a much clearer critical current developing in the parallel direction than in the perpendicular direction.

B. Model-*B* disorder

To study model-*B* disorder, we consider an $8 \times 8 \times 5$ lattice with flux per plaquette $f = \frac{1}{8}$, parallel to the z (thin) direction. We have considered three types of defect configurations: (i) "point defects," introduced by removing at random 40 grains, and their associated Josephson couplings (but not shunt resistances) from among the 320 grains of the lattice; (ii) "random line defects," consisting of eight line defects, each five grains long, parallel to the z direction but randomly distributed in the xy plane; and (iii) "periodic line defects," in which the line defects are arranged with the periodicity of the ground-state phase configuration at $f = \frac{1}{8}$. For reference, we also consider (iv) the no-defect configuration.

In the absence of an applied current, the phases of configuration (iv) will settle into a z-independent ground-state configuration. This can be found numerically, e.g., by starting the phases in a random arrangement and iterating the Josephson equations at zero applied current until a state of no voltage is obtained (care must be exercised to avoid falling into a metastable minimum). To calculate the *IV* characteristics, we typically begin with this ground state, gradually increasing the applied current for various defect configurations.

Figure 8 shows the resulting *IV* characteristics (for **J⊥B**) at temperature $T = 0$. Case (iv) has a critical current $\approx 0.12 I_c$ per junction, comparable to the calculated depinning critical current for a single vortex in a large square array.[28] This suggests that the critical current is not too much influenced, in this case, by vortex-vortex interactions. The critical current is increased slightly by point defects [case (i)], somewhat more by random line defects [case (ii)], and considerably more again by periodic line defects [case (iii)]. In case (ii), the functional form of the *IV* characteristic is considerably modified by the defects (being concave up rather than concave down). We find that it is fairly well fitted

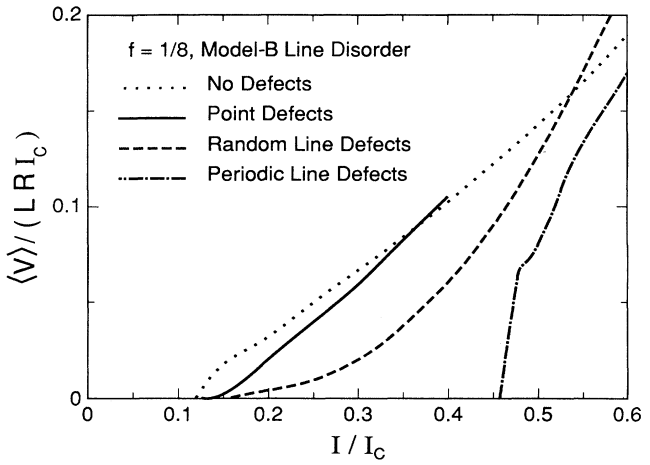

FIG. 8. IV characteristics for model-B disorder and $\mathbf{J}\perp\mathbf{B}$, at temperature $T=0$, and $L\times L\times L_z$ array, with $L=8$, $L_z=5$, magnetic flux $f=\frac{1}{8}$ with $\mathbf{B}$ parallel to the z (thin) direction: no defects (dotted curve); 40 randomly distributed point defects (full curve, average of seven realizations); eight randomly distributed line defects parallel to the z direction (dashed curve, average of ten realizations); and eight periodically distributed line defects in the z direction (dot-dashed curve). I is the applied current per grain; $\langle V\rangle$ is the time-averaged voltage across the sample, averaged over the directions perpendicular to the current; R is the shunt resistance, and I_c is the critical current of each junction. For reference, the critical current for the ordered lattice at $f=0$ is $I/I_c=1.0$.

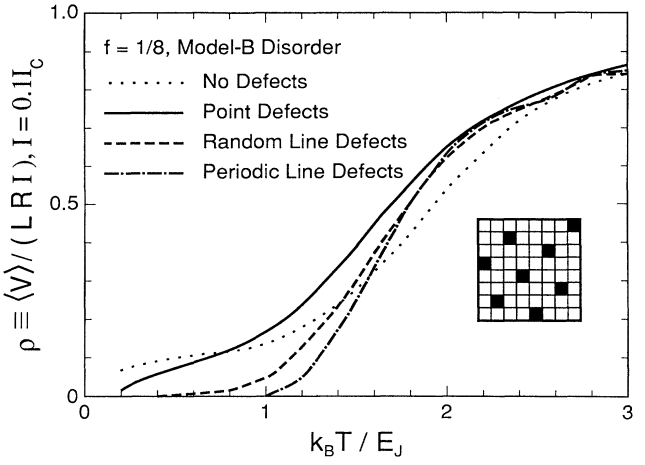

FIG. 9. Resistivity $\rho(T)\equiv V/I$, at an applied current $I=0.1I_c$ per junction, plotted vs temperature T, at $f=\frac{1}{8}$. Symbols as in Fig. 10. Inset: ground-state vortex line configuration for $f=\frac{1}{8}$ lattice. Filled squares denote loci of vortex lines (plaquettes of positive vorticity, i.e., current circulating counterclockwise); empty squares are plaquettes of negative vorticity. For reference, $T_c(f=0)\approx 2.21E_J/k_B$.

by $\langle V\rangle/(LRI_c)=A\exp[-C(I_c/I)^{\mu}]$ with $\mu\approx 0.3$, $A\approx 3\times 10^4$, and $C\approx 10$.

Figure 9 shows the temperature-dependent resistivity $\rho(T)\equiv V/I$ at a current of $0.1I_c$ per junction, for cases (i)–(iv) and $\mathbf{J}\perp\mathbf{B}$. For reference, the superconducting transition temperature $T_c(B=0)$ of the Hamiltonian (1) in zero magnetic field and zero current is known to occur at $k_BT_c\approx 2.21E_J$.[29] Hence Fig. 9 suggests that, whatever the defects, $T_c(f=\frac{1}{8})<T_c(f=0)$—that is, as expected, T_c is reduced in a magnetic field. However, relative to the zero-defect case, $T_c(\frac{1}{8})$ is increased slightly by point defects, more yet by random line defects, and still more by periodically arranged line defects. The increase in $T_c(\frac{1}{8})$ produced by random line defects corresponds to the increase in the "irreversibility temperature" observed by Civale *et al.* when random line defects are introduced parallel to the magnetic field. Note that, in Fig. 9, the density of line defects "equals" the density of point defects in the sense that an equal amount of superconducting material is removed in each case. The only difference among the various defect curves in Fig. 9 is the degree to which the disorder is correlated. Hence this plot provides a very direct illustration of the influence of correlation in raising the "irreversibility temperature."

Figure 10 shows the $T=0$ IV characteristics for a flux density $f=\frac{1}{8}$ and several densities f_d of randomly distributed line defects. Figure 11 shows a similar plot for $\rho(T)$ at a current level of $0.1I_c$. These figures suggest that (at least for $f=\frac{1}{8}$) both the $T=0$ critical current and $T_c(B)$ are largest when $f\approx f_d$, a conclusion which may qualitatively agree with experiment.[8] To confirm these conclusions, however, Monte Carlo calculations should be carried out on the analogous Hamiltonian to determine the dependence of T_c on defect line density preferably for much larger samples.

To summarize for model-B disorder, our results suggest that columnar defects oriented parallel to the flux lines tend to increase the critical current, and to push up the superconducting transition temperature $T_c(B)$, relative to the same number of random point defects at the same field, in apparent agreement with experiment. We find also that a periodic arrangement of line defects com-

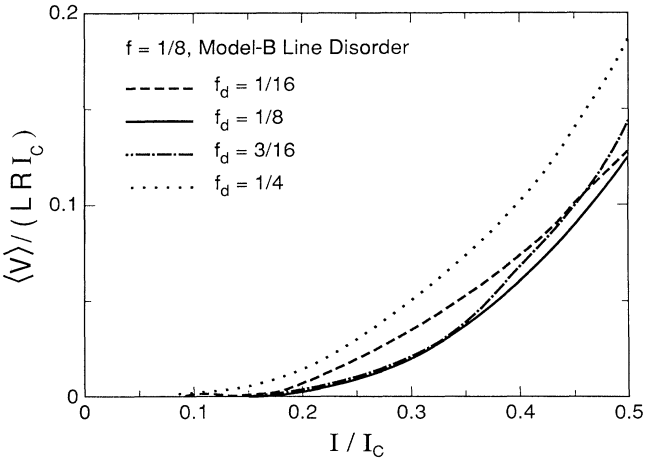

FIG. 10. Same as Fig. 8, but for a flux $f=\frac{1}{8}$ and several densities f_d of columnar defects oriented parallel to the z axis. Each curve represents an average over ten realizations of the disorder. In this case, the lattice is $8\times 8\times 8$.

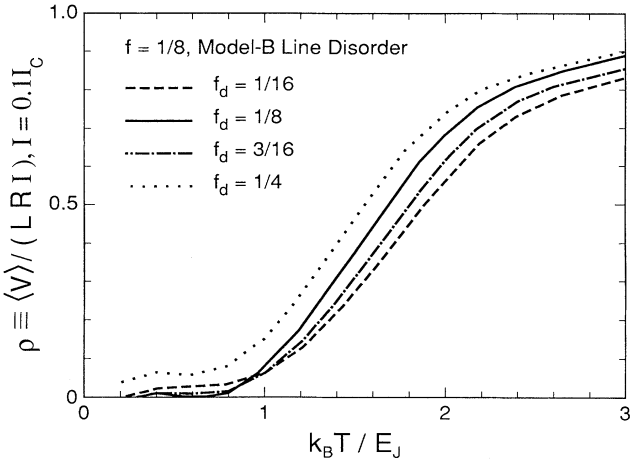

FIG. 11. Same as Fig. 9, but for a flux $f = \frac{1}{8}$ and several densities f_d of columnar defects oriented parallel to the z axis. Each curve represents an average over ten realizations of the disorder.

mensurate with the defect-free flux lattice is even more effective in increasing both the critical current and $T_c(B)$. Finally, we have preliminary evidence that the pinning (and T_c-enhancing) effects of random line defects are optimized when the defect density is comparable to the flux density.

IV. DISCUSSION

Nelson and Vinokur[22] have recently proposed a theory of the superconducting transition in materials with correlated disorder. When the density of line defects is greater than the density of flux lines, their theory leads to a phase transition from a high-temperature flux liquid into a low-temperature "Bose-glass" phase. In their theory, the three-dimensional superconductor maps onto a two-dimensional system in which the flux lines play the lines of interacting Bose particles while the line defects become static point defects. When the density of line defects equals the density of flux lines, Nelson and Vinokur predict instead a transition into a "Mott insulator" phase, in which the flux lines are localized on the line defects.

Although our numerical samples are simply too small to test this picture (and although our models, which have long-range interactions between the vortex lines, may be in a different universality class from the Bose-glass model), we briefly interpret our results in the context of this theory. The "Bose-glass" regime, in which the line defect density $f_d > f$, corresponds to our model A and one of the cases considered in our model B. In this regime, for $T < T_c(B)$, Vinokur and Nelson predict a nonlinear IV relation of the form $V/J \propto \exp[-(E_k/k_B T)(J_0/J)^{1/3}]$ where J is the current density and E_k and J_0 are constants depending on the strength of the pinning potential and other parameters. Our IV characteristics for model A (with $\mathbf{J} \perp \mathbf{B}$) are at least consistent with this behavior. For $\mathbf{J} \perp \mathbf{B}$, a simple activation form ($V/J \propto \exp[-E_k J^0/(J k_B T)]$) seems unlikely on the basis of our results; however, we are not aware of an analytical theory describing Bose-glass transport in this regime. Obviously, more detailed numerical simulations, involving much larger numbers of line defects and more disorder realizations, are needed before any definite conclusions can be drawn about the applicability of the Bose glass picture to this dynamical model.

Our results for model-A disorder may be consistent with static and dynamic scaling hypotheses as applied to this anisotropic phase transition, but our numerical results are not sufficient to make reliable estimates of the relevant critical indices. It appears that the anisotropy exponent z may lie between 1 and 2, which is in the range of findings for other lattice models with line disorder,[30] and may be smaller than that found in analogous calculations with short-range interactions[27] between vortex lines, for which $z = 2$. Our dynamical results leave open the possibility that there is only a single dynamical exponent z' for transport both perpendicular and parallel to the line defects, in contrast to the short-range model. This conclusion may, however, be a function of the particular dynamics assumed in our calculations.[31]

To summarize, we have studied flux pinning by defects in three-dimensional Josephson-junction networks with various types of point and line defects. We find that line defects considerably enhance both the critical current and the upper critical field, relative to the same concentration of point defects. We also find some indications that the normal-to-superconducting transition in the case of random line disorder is a continuous phase transition marked by both static and dynamical critical phenomena. These conclusions are, however, subject to large numerical uncertainties arising from the relatively small samples studied. The results may be applicable to high-T_c superconductors in which the intrinsic anisotropy is not too great (such as $YBa_2Cu_3O_{7-\delta}$) and if screening fields can be neglected (extreme type-II limit). Larger scale calculations, including screening, and making use of more realistic pinning models, will be necessary for quantitative comparisons to experiment. These are planned for future work.

ACKNOWLEDGMENTS

We should like to thank M. P. A. Fisher, D. A. Huse, M. Makivic, D. R. Nelson, Mats Wallin, and A. P. Young for many useful conversations. This work has been supported by the Midwest Superconductivity Consortium (MISCON) through Department of Energy Grant No. DE-FG02-90ER45427, and in part by NSF Grant No. DMR 90-20994. Calculations were carried out on the Cray Y-MP 8/864 of the Ohio Supercomputer Center.

APPENDIX A: STATIC SCALING

We describe our numerical results for line defects within the framework of a scaling analysis suitable for both our static and dynamic results, based largely on previous discussions of Nelson and Vinokur.[22] In this appendix, we describe the static scaling hypotheses.

Consider a HTSC with line defects and a magnetic field both oriented in the z direction. Suppose that there is a phase transition at some temperature $T_c(B)$, where B is the magnitude of the applied magnetic field. Assume also that this phase transition is characterized by *two* diverging correlation lengths, $\xi_\perp$ and $\xi_\parallel$, corresponding to correlations in the xy plane and z direction, respectively. To allow for the possibility that these diverge with different critical exponents, we write

$$\xi_\perp \propto t^{-\nu_\perp} , \tag{A1}$$

$$\xi_\parallel \propto t^{-z\nu_\perp} , \tag{A2}$$

$$t = |T - T_c(B)| / T_c(B) . \tag{A3}$$

An isotropic phase transition is a special case of this behavior with $z = 1$.

By analogy with the usual isotropic hyperscaling expression for the singular part f_s of the free energy density near T_c, we assume that f_s behaves as

$$\beta f_s \propto \frac{1}{\xi_\perp^2 \xi_\parallel} \tag{A4}$$

(where $\beta = 1/k_B T$). Hence the specific heat has a singularity of the form

$$C_V \propto \frac{\partial^2 f}{\partial t^2} \propto t^{\nu_\perp(2+z)-2} . \tag{A5}$$

To estimate the behavior of $\gamma_\perp$ and $\gamma_\parallel$, the principal components of the helicity modulus tensor, we extend an argument of Cha *et al.*[24] to anisotropic phase transitions. First imagine that the array is subjected to a phase gradient $\nabla_z \theta$ in the z direction. The change in free energy per unit volume is

$$\beta f_s \propto \tfrac{1}{2}\gamma_\parallel |\nabla_z \theta|^2 \propto \frac{\gamma_\parallel}{\xi_\parallel^2} , \tag{A6}$$

where we have replaced ∇_z by the inverse of the characteristic length $\xi_\parallel$. With the use of Eqs. (A2) and (A4), this gives

$$\gamma_\parallel \propto \frac{\xi_\parallel}{\xi_\perp^2} \propto t^{(2-z)\nu_\perp} , \tag{A7}$$

where the last proportionality describes the expected critical behavior near T_c. A similar argument applied to $\gamma_\perp$ gives

$$\gamma_\perp \propto \frac{1}{\xi_\parallel} \propto t^{z\nu_\perp} . \tag{A8}$$

In a Monte Carlo calculation, it is necessary to calculate these quantities in finite-size samples, usually a parallelopiped of volume $L_\perp^2 L_\parallel$. The natural scaling form for the helicity moduli in such samples is

$$\gamma_\perp = \frac{1}{\xi_\parallel} F(\xi_\parallel/L_\parallel, \xi_\perp/L_\perp) , \tag{A9}$$

$$\gamma_\parallel = \frac{\xi_\parallel}{\xi_\perp^2} G(\xi_\parallel/L_\parallel, \xi_\perp/L_\perp) , \tag{A10}$$

where $F(u,v)$ and $G(u,v)$ are universal functions. Expressions (A9) and (A10) can be written in more convenient forms by making the change of variables $F(u,v) = uH(uv^{-z}, u)$, $G(u,v) = (v^2/u)K(uv^{-z}, u)$ to yield

$$\gamma_\perp = \frac{1}{L_\parallel} H(L_\perp^z/L_\parallel, L_\parallel/\xi_\parallel) , \tag{A11}$$

$$\gamma_\parallel = \frac{L_\parallel}{L_\perp^2} K(L_\perp^z/L_\parallel, L_\parallel/\xi_\parallel) . \tag{A12}$$

At $T = T_c$, the second argument of both H and K vanishes. Hence, for a finite sample whose dimensions are chosen such that $L_\parallel \propto L_\perp^z$, it follows that

$$L_\parallel \gamma_\perp = \text{const} , \tag{A13}$$

$$L_\perp^2 \gamma_\parallel / L_\parallel = \text{const} . \tag{A14}$$

These relations can, in principle, be used to determine the transition temperature with high accuracy by examining the behavior of the components of γ in a series of boxes of different volumes, such that the ratio $L_\parallel/L_\perp^z$ is held constant. The method is to plot $L_\parallel \gamma_\perp$ and $L_\perp^2 \gamma_\parallel / L_\parallel$ for different volumes; all should cross at $T = T_c$. Unfortunately, this method works only provided z is known. Since z is apparently in the range 1.2–1.5 for the present model, but difficult to determine with greater accuracy, we have not attempted this kind of anisotropic finite-size scaling in the present paper.

APPENDIX B: DYNAMIC SCALING

For dynamical quantities, we may again follow and somewhat extend the arguments of Nelson and Vinokur.[22] We consider first the electric field $E_\perp$ and current density $J_\perp$ in the transverse direction. In this case, we postulate a scaling relation of the form

$$E_\perp = \xi_\perp^{-a} E_{\pm,\perp}(\hbar J \xi_\perp \xi_\parallel / (2ek_B T)) , \tag{B1}$$

where $E_{\pm,\perp}$ are scaling functions which apply, respectively, above and below T_c. To determine a, suppose the HTSC is in the Ohmic regime at $T > T_c$. In this regime, $E_{+,\perp}(x) \propto x$, whence $\sigma_\perp \equiv J_\perp/E_\perp \propto \xi_\perp^{a-1-z}$. However, we also expect that $\sigma_\perp$ should scale like $\gamma_\perp/\omega$ (that is, both of these quantities should have the same power-law dependence on $\xi_\perp$, where ω is a characteristic frequency). In turn, we expect that ω should vanish near this continuous phase transition, with a characteristic temperature dependence given by $\xi_\perp^{-z'}$ where z' is a new dynamical critical exponent. Combining all these relations, and using Eq. (A8), we obtain

$$a = 1 + z' . \tag{B2}$$

Similarly, for transport parallel to the z axis, we expect the scaling relation

$$E_\parallel = \xi_\perp^{-b} E_{\pm,\parallel}(\hbar J_\parallel \xi_\perp^2 / (2ek_B T)) , \tag{B3}$$

and making arguments analogous to the perpendicular case, we find

$$b = z + z' \ . \tag{B4}$$

Precisely at $T = T_c$ we expect both $E_\perp$ and $E_\parallel$ to vary as power laws in $J_\perp$ and $J_\parallel$, respectively. This behavior implies that at T_c the scaling functions $E_{\pm,\perp}(x)$ and $E_{\pm,\parallel}(x)$ should take the forms

$$E_{\pm,\perp}(x) \propto x^c \ , \tag{B5}$$

$$E_{\pm,\parallel}(x) \propto x^d \ . \tag{B6}$$

The exponents c and d can be determined by observing that $\xi_\perp$ and $\xi_\parallel$ are infinite at T_c. In order for Eqs. (B1) and (B3) still to be satisfied at T_c, the left- and right-hand sides must involve equal powers of t. This leads to the results

$$c = (1+z')/(1+z) \ , \tag{B7}$$

$$d = (z+z')/2 \ . \tag{B8}$$

Thus, calculating or measuring the current-voltage characteristics precisely at $T = T_c$ should yield power laws whose slopes determine the exponents z and z'.

The above arguments assume that there is a single dynamical critical exponent z'. If instead, there are two such exponents $z'_\perp$ and $z'_\parallel$ describing the divergent relaxation times in the perpendicular and parallel directions, then Eqs. (B7) and (B8) are replaced by the relations $c = (1+z'_\perp)/(1+z)$; $d = (z+z'_\parallel)/2$.

APPENDIX C: DYNAMICAL SCALING IN FINITE-SIZE SYSTEMS

Our finite-size IV characteristics often show an Ohmic tail at low currents, even at temperatures well below the putative superconducting transition. In this appendix, we give an argument suggesting that this tail is a finite-size effect which would disappear in sufficiently large systems.

We present the argument for the case $J \| B$, where the numerical results most clearly show the finite-size tail. However, a similar argument should also hold for the perpendicular case. In the parallel case, for $T < T_c$ in an infinite system as shown in Appendix B, the electric field and current density are related by

$$E_\parallel = \xi_\perp^{-(z+z')} E_{-,\parallel}(\hbar J_\parallel \xi_\perp^2/(2ek_BT)) \ , \tag{C1}$$

where E_- is some universal function. Now write $E_{-,\parallel}(x) = xF_{-,\parallel}(x)$. It follows that the resistivity $\rho_\parallel \equiv E_\parallel / J_\parallel$ can be written as

$$\rho_\parallel \propto \xi_\parallel^{2-z-z'} F_{-,\parallel}(\hbar J_\parallel \xi_\perp^2/(2ek_BT)) \ . \tag{C2}$$

For a cubic system of edge L, this relation must involve another variable, the ratio $\xi_\perp/L$:

$$\rho_\parallel \propto \xi_\perp^{2-z-z'} F_{-,\parallel}(\hbar J_\parallel \xi_\perp^2/(2ek_BT), \xi_\perp/L) \ . \tag{C3}$$

The numerical data presented in Fig. 7(b) suggest that $F_{-,\parallel}(x,0)$ falls rapidly to zero with decreasing x. Indeed, the data seem to fit roughly to the relation

$$F_{-,\parallel}(x,0) = F_0 \exp(-A/x^{\mu_\parallel}) \ , \tag{C4}$$

where F_0 and A are constants and $\mu_\parallel \approx 1$. We have no theory for the finite-size version of this function, but a plausible guess suggests itself. The dimensionless argument $x = \hbar J_\parallel \xi_\perp^2/(2ek_BT)$ may be expressed as $x = (\xi_\perp/\xi_J)^2$ where $\xi_J = [2ek_BT/(\hbar J_\parallel)]^{1/2}$ is a characteristic length defined by the current density $J_\parallel$ (note that length is measured in units of the intergranular separation). When this length becomes larger than the system size, the current length should be replaced by L. In order to include this behavior in the scaling form, we may postulate

$$F_{-,\parallel}(\hbar J_\parallel \xi_\perp^2/(2ek_BT), \xi_\perp/L) = F_0 \exp\left[\frac{-A}{[\hbar J_\parallel \xi_\perp^2/(2ek_BT) + \xi_\perp^2/L^2]^{\mu_\parallel}} \right] \ . \tag{C5}$$

This function has several desirable properties. First, for large L, it reduces to the infinite-size form of Eq. (C4). Secondly, for very small $J_\parallel$, $\rho_\parallel$ becomes independent of $J_\parallel$ (i.e., becomes Ohmic) and is given by

$$\rho_\parallel \propto \xi_\parallel^{2-z-z'} \exp(-AL^{2\mu_\parallel}/\xi_\parallel^{2\mu_\parallel}) \ . \tag{C6}$$

Equation (C6) is the desired low-current Ohmic tail seen in our calculations. As expected, it goes away at large enough sizes, or low enough temperatures ($\xi_\parallel$ becomes smaller and smaller as the temperature is decreased below T_c). Since $z + z' \approx 4-5$, the prefactor in Eq. (C3) grows with decreasing temperature. However, its growth should be more than offset by the decreasing exponential, so that $\rho_\parallel$ should decrease with decreasing temperature for fixed large L. Thus the argument presented in this appendix gives a plausible explanation of the finite-size numerical results discussed in the text.

[1]For recent references on critical currents in high-temperature superconductors, see, e.g., L. N. Bulaevskii, J. R. Clem, L. I. Glazman, and A. P. Malozemoff, Phys. Rev. B **45**, 2545 (1992), and references therein.

[2]P. W. Anderson, Phys. Rev. Lett. **8**, 309 (1962).

[3]Y. B. Kim, Rev. Mod. Phys. **36**, 39 (1964).

[4]M. R. Beasley, R. Labusch, and W. W. Webb, Phys. Rev. **181**, 682 (1969).

[5]A. M. Campbell and J. E. Evetts, Adv. Phys. **21**, 199 (1972).

[6]Y. Yeshurun and A. P. Malozemoff, Phys. Rev. Lett. **60**, 2202 (1988).

[7]For a recent discussion of flux flow in high-temperature superconductors, see, e.g., A. P. Malozemoff, T. K. Worthington, E. Zeldov, N. C. Yeh, M. W. McElfresh, and F. Holtzberg, in *Strong Correlations and Superconductivity,* edited by H. Fukuyama, S. Maekawa, and A. P. Malozemoff, Springer Series in Solid State Sciences Vol. 89 (Springer-Verlag, Heidelberg, 1989), p. 349.

[8]L. Civale, A. D. Marwick, T. K. Worthington, M. A. Kirk, J. R. Thompson, L. Krusin-Elbaum, Y. Sun, J. R. Clem, and F. Holtzberg, Phys. Rev. Lett. **67**, 648 (1991).

[9]See, e.g., L. Civale, A. D. Marwick, M. W. McElfresh, T. K. Worthington, A. P. Malozemoff, F. Holtzberg, J. R. Thompson, and M. A. Kirk, Phys. Rev. Lett. **65**, 1164 (1990).

[10]R. B. Van Dover, E. M. Gyorgy, L. F. Schneemeyer, J. W. Mitchell, K. V. Rao, R. Puzniak, and J. V. Waszczak, Nature (London) **342**, 55 (1989).

[11]F. M. Sauerkopf, H. P. Wiesinger, H. W. Weber, G. W. Crabtree, and J. Z. Liu, Physica (The Hague) **162-164C**, 751 (1989).

[12]K. A. Muller, M. Takashige, and J. Bednorz, Phys. Rev. Lett. **58**, 1143 (1987).

[13]Some representative references are K. K. Mon and S. Teitel, Phys. Rev. Lett. **62**, 673 (1989); W. Xia and P. L. Leath, *ibid.* **63**, 1428 (1989); K. H. Lee, D. Stroud, and J. S. Chung, *ibid.* **64**, 962 (1990); F. Falo, A. R. Bishop, and P. S. Lomdahl, Phys. Rev. B **41**, 10 983 (1990); H. Eikmans and J. E. van Himbergen, *ibid.* **41**, 8927 (1990); J. U. Free, S. P. Benz, M. S. Rzchowski, M. Tinkham, C. J. Lobb, and M. Octavio, *ibid.* **41**, 7267 (1990); L. I. Sohn, M. S. Rzchowski, J. U. Free, S. P. Benz, M. Tinkham, and C. J. Lobb, *ibid.* **44**, 925 (1992); D. Dominguez, J. V. Jose, A. Karma, and C. Wiecko, Phys. Rev. Lett. **67**, 2367 (1991); J. S. Chung, K. H. Lee, and D. Stroud, Phys. Rev. B **40**, 6570 (1989); W. Yu, K. H. Lee, and D. Stroud, *ibid.* **47**, 5906 (1993).

[14]See, e.g., M. Tinkham and C. J. Lobb, in *Solid State Physics: Advances in Research and Applications,* edited by H. Ehrenreich and D. Turnbull (Academic, New York, 1989), Vol. 42, p. 91.

[15]K. H. Lee and D. Stroud, Phys. Rev. B **46**, 5699 (1992).

[16]J. D. Reger, T. A. Tokuyasu, A. P. Young, and M. P. A. Fisher, Phys. Rev. B **44**, 7147 (1991).

[17]W. Y. Shih, C. Ebner, and D. Stroud, Phys. Rev. B **30**, 134 (1984).

[18]V. Ambegaokar and B. I. Halperin, Phys. Rev. Lett. **22**, 1364 (1968).

[19]D. Arovas and F. D. M. Haldane (unpublished).

[20]R. E. Prange, in *The Quantum Hall Effect,* 2nd ed., edited by R. E. Prange and S. M. Girvin (Springer-Verlag, New York, 1990), Chap. 1.

[21]R. E. Hetzel, A. Sudbo, and D. A. Huse, Phys. Rev. Lett. **68**, 518 (1992), have studied a similar model on a simple hexagonal lattice, for which, unlike the present model, the underlying triangular Abrikosov flux lattice is unfrustrated at certain values of f. For sufficiently small f (approximately $f<\frac{1}{6}$) they find a *first*-order melting transition, in apparent contrast to our results for $f=\frac{1}{4}$ on a simple cubic lattice.

[22]D. R. Nelson and V. M. Vinokur, Phys. Rev. Lett. **68**, 2398 (1992).

[23]D. S. Fisher, M. P. A. Fisher, and D. A. Huse, Phys. Rev. B **43**, 130 (1991).

[24]M.-C. Cha, M. P. A. Fisher, S. M. Girvin, M. Wallin, and A. P. Young, Phys. Rev. B **44**, 6883 (1991).

[25]A somewhat similar isotropic model, but for point disorder, has been introduced by D. A. Huse and H. S. Seung [Phys. Rev. B **42**, 1059 (1990)], and studied by Monte Carlo simulations (see also Ref. 16). Dynamic simulations for that model have been carried out by K. H. Lee and D. Stroud, Phys. Rev. B **44**, 9780 (1991).

[26]J. T. Chayes, L. Chayes, D. S. Fisher, and T. Spencer, Phys. Rev. Lett. **57**, 2999 (1986).

[27]M. Wallin and S. M. Girvin, Phys. Rev. B **47**, 14 642 (1993).

[28]See, e.g., C. J. Lobb, D. Abraham, and M. Tinkham, Phys. Rev. B **27**, 150 (1983).

[29]M. Ferer, M. A. Moore, and M. Wortis, Phys. Rev. B **8**, 5205 (1973).

[30]D. Andelman and A. Aharony, Phys. Rev. B **31**, 4305 (1985).

[31]The same dynamics have been used to study the phase transition at $f=0$ in the absence of defects [K. H. Lee and D. Stroud, Phys. Rev. B **46**, 5699 (1992)], with a resulting dynamical exponent $z'\approx 1.5$. This agrees with expectations for so-called model-F dynamics [P. Hohenberg and B. I. Halperin, Rev. Mod. Phys. **49**, 435 (1977)], to which we believe our overdamped Josephson equations correspond.